The EMBO Journal (2010) 29, 3911–3923 | © 2010 European Molecular Biology Organization | All Rights Reserved 0261-4189/10
www.embojournal.org

THE EMBO JOURNAL

Direct observation of stepped proteolipid ring rotation in *E. coli* F_oF_1-ATP synthase

Robert Ishmukhametov[1], Tassilo Hornung[1], David Spetzler[1] and Wayne D Frasch*

Faculty of Biomedicine and Biotechnology, School of Life Sciences, Arizona State University, Tempe, AZ, USA

Although single-molecule experiments have provided mechanistic insight for several molecular motors, these approaches have proved difficult for membrane bound molecular motors like the F_oF_1-ATP synthase, in which proton transport across a membrane is used to synthesize ATP. Resolution of smaller steps in F_o has been particularly hampered by signal-to-noise and time resolution. Here, we show the presence of a transient dwell between F_o subunits a and c by improving the time resolution to 10 μs at unprecedented S/N, and by using *Escherichia coli* F_oF_1 embedded in lipid bilayer nanodiscs. The transient dwell interaction requires 163 μs to form and 175 μs to dissociate, is independent of proton transport residues aR210 and cD61, and behaves as a leash that allows rotary motion of the c-ring to a limit of ~36° while engaged. This leash behaviour satisfies a requirement of a Brownian ratchet mechanism for the F_o motor where c-ring rotational diffusion is limited to 36°.

The EMBO Journal (2010) **29,** 3911–3923. doi:10.1038/emboj.2010.259; Published online 29 October 2010
Subject Categories: membranes & transport; cellular metabolism
Keywords: Brownian ratchet mechanism; F_oF_1-ATP synthase; gold nanorods; nanodiscs; single-molecule measurements

Introduction

The F_oF_1-ATP synthase is composed of two opposed rotary molecular motors connected by a common axle of γε-subunits (Stock *et al*, 1999). The integral membrane F_o motor, which has a subunit stoichiometry of ab_2c_{10} in *Escherichia coli* (Jiang *et al*, 2001), uses the electrochemical potential-driven flux of protons across a membrane (proton-motive force (PMF)) to drive clockwise rotation of the ring of 10 c-subunits as viewed from the periplasm (Börsch *et al*, 2002). The c-ring is docked to the γε-subunits that extend into the hexameric ring of α- and β-subunits in the F_1 peripheral membrane motor. Rotation of this axle drives conformational changes in each of the three catalytic αβ heterodimers resulting in ATP synthesis (Boyer, 1997). The F_1 motor can also hydrolyze ATP resulting in counterclockwise γε-subunit rotation and proton translocation via F_o (Börsch *et al*, 2002).

*Corresponding author. School of Life Sciences, Arizona State University, Box 874501, Tempe, AZ 85287 USA. Tel.: +1 480 965 8663; Fax: +1 480 965 6899; E-mail: frasch@asu.edu
[1]These authors contributed equally to this work

Received: 19 April 2010; accepted: 21 September 2010; published online: 29 October 2010

When solubilized away from F_o and the membrane, *E. coli* F_1-ATPase-driven rotation at saturating ATP concentrations occurs in three 120° power strokes (Sabbert *et al*, 1996; Noji *et al*, 1999; Spetzler *et al*, 2006), separated by 8.3 ms dwells comparable to the turnover time of the rate-limiting step of ATP hydrolysis (Spetzler *et al*, 2006; Hornung *et al*, 2008). In the absence of drag on the F_1 motor, the velocity of the power stroke is $\sim 0.5^\circ\,\mu s^{-1}$ (Spetzler *et al*, 2006).

In vivo, F_oF_1 uses the PMF across the membrane to maintain the [ATP]/[ADP][Pi] ratio (Q) far from equilibrium so that the high-ATP concentration provides an energy source to drive other cellular processes. Energetically, this means that at steady state, cellular PMF ≅ 2.3RTlogQ. In other words, the driving force of the F_o motor (PMF) is in equilibrium with the driving force of the F_1 motor (logQ). In *E. coli*, the cytoplasm typically contains 3 mM ATP, 0.4 mM ADP, and 6 mM Pi such that logQ ≅ 0.1 (Weber and Senior, 1997).

The maximum reported rate of *E. coli* F_oF_1 ATP synthesis (Senior *et al*, 2002) is about $100\,s^{-1}$ ($10\,ms\ ATP^{-1}$), although rates of $27\,s^{-1}$ ($37\,ms\ ATP^{-1}$) are more common with *E. coli* F_oF_1 in proteolipisomes (Fischer *et al*, 1994). Proton translocation can occur at faster rates when powered by ATP hydrolysis (Feniouk and Junge, 2008), or by membrane potentials imposed on *E. coli* F_o-embedded membranes after removal of F_1 (Franklin *et al*, 2004; Wiedenmann *et al*, 2008). In the absence of F_1 there is no indication that the proton translocation rate of F_o saturates at high-driving force (Feniouk and Junge, 2008), which suggests that the proton translocation step is not rate limiting to the mechanism.

Proton translocation across the membrane occurs in F_o when subunit-a residue aR210 deprotonates the cD61 carboxyl on each c-subunit as the c-ring rotates (Fillingame *et al*, 1984; Lightowlers *et al*, 1987; Angevine *et al*, 2003; Ishmukhametov *et al*, 2008). A Brownian ratchet mechanism has been postulated to power F_o rotation that must meet two requirements to function (Junge *et al*, 1997; Oster *et al*, 2000): first, that there are two noncolinear proton access half-channels from each side of the membrane leading to the cD61 carboxyl; and second, that rotational diffusion of the c-ring relative to subunit-a is periodically restricted in some manner. However, experimental evidence that provides a molecular basis for the latter requirement is scarce.

Initial single-molecule c-ring rotation measurements of F_oF_1 driven by ATP hydrolysis, or by an electrochemical potential, resolved only 120° steps (Sambongi *et al*, 1999; Pänke *et al*, 2000; Börsch *et al*, 2002; Kaim *et al*, 2002; Nishio *et al*, 2002; Ueno *et al*, 2005). C-ring rotation with step sizes of 36°, 72°, 108°, and 144° occurring 48, 37, 12, and 3% of the time, respectively, have now been observed using *E. coli* F_oF_1 proteoliposomes that synthesized an ATP every 37 ms in response to a membrane potential of >200 mV (Düser *et al*, 2009). As the proton translocation rate of F_o does not saturate at high-driving force (Feniouk and Junge, 2008), the movement of c-subunits past subunit-a during the 72°, 108°, and 144° steps may not have caused a dwell in rotation.

We now report the observation of a previously unknown interaction between F_o subunits a and c of F_oF_1 when ATPase-driven rotation is slowed by a viscosity-induced load. A striking feature of this interaction is that it forms a leash that limits rotation to $\sim 36^\circ$ in a manner that can satisfy the restricted motion requirement in the F_o Brownian ratchet mechanism. As the transient dwells do not form when c-ring rotation and proton transport occur at high rates, the practical advantage of using the leash is anticipated to be under steady-state conditions in which the cellular ATP concentration is high relative to ADP and Pi. Under these conditions, when the free energy of the proton gradient approaches equilibrium with the chemical potential of ATP, the F_o motor could use this leash as part of a Brownian ratchet to bias rotation for ATP synthesis (clockwise) against an F_1 motor-imposed load.

Results

F_oF_1 nanodiscs are fully assembled and retain complete activity during single-molecule measurements

To stabilize the hydrophobic F_o complex, we inserted solubilized F_oF_1 into phospholipid bilayer nanodiscs. The particle size of nanodiscs is constrained by the membrane scaffold protein (MSP) construct MSP-1E3D1 that forms a 13-nm diameter ring of α-helices around a bilayer of phospholipid molecules, and has been shown to provide a good model for lipid bilayers (Bayburt *et al*, 2007). The nanodiscs are large enough to allow the incorporation of the F_o complex and a few hundred lipid molecules, yet are on the same scale as the F_oF_1 complex. Assembly of stable nanodisc-F_oF_1 complexes (n-F_oF_1) from MSP, lipids, and detergent solubilized F_oF_1 was verified by 2D electrophoresis (Figure 1). The first nondenaturing gel dimension contained one prominent band. This band contained both MSP and the F_oF_1 subunits when separated in the second denaturing gel dimension. The absence of other bands in the nondenaturing gel corresponding to incomplete n-F_oF_1 constructs suggests that the majority of proteins contain the full complement of subunits.

We made the c2∇C mutation to a cys-free *E. coli* F_oF_1 enzyme that inserted a sulfhydryl group on each c-subunit for covalent modification with biotin maleimide, which is designated here as F_oF_1. Figure 1C shows the ATPase activity of n-F_oF_1 versus detergent solubilized F_oF_1 as a function of time. Detergent solubilized F_oF_1 lost all activity and aggregated within a few hours at room temperature. In comparison, the activity of n-F_oF_1 was initially higher and did not decline significantly after the preparation had been at 25° for 8 h. Modification of cD61 in the c-ring of n-F_oF_1 by *N*,*N*′-dicyclohexylcarbodiimide (DCCD) inhibited ATPase activity by as much as 85% (Table I), indicating that there was strong coupling between hydrolysis and proton transport. This extent of inhibition is comparable to that reported by Ueno *et al* (2005) for detergent solubilized F_oF_1 used in single-molecule rotation studies. The rapid loss of activity of detergent solubilized enzyme may explain why Ueno *et al* (2005) observed rotation of only 60 detergent solubilized F_oF_1 molecules in 840 fields of view.

Biotinylated n-F_oF_1 was attached to a cover slip via 6xHis-tags on the β-subunit N-terminus. Subsequent addition of avidin-coated gold nanorods then became bound to the biotins positioned on the c-ring distal from F_1 (Figure 2A).

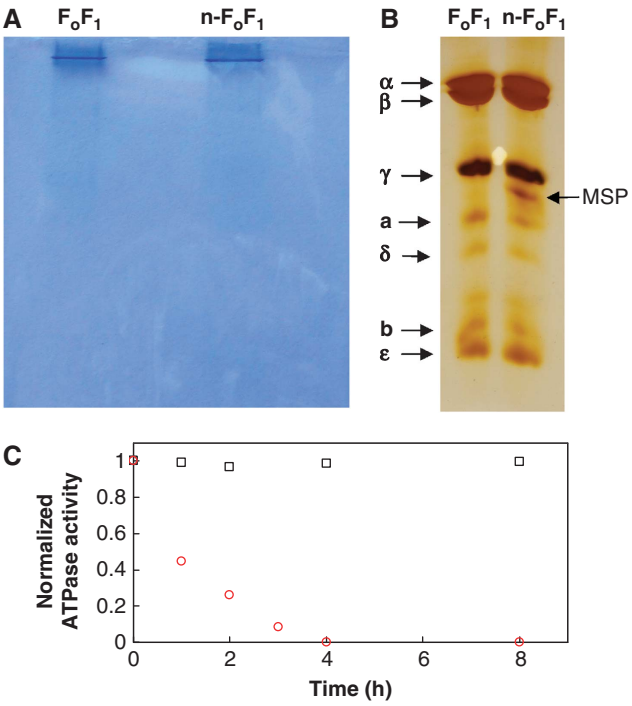

Figure 1 Incorporation of F_oF_1 into nanodiscs. Two-dimensional electrophoresis gel of purified F_oF_1 before (left lane) and after (right lane) incorporation into nanodiscs. (**A**) Dimension 1: Coomassie-stained 5–15% nondenaturing gel. (**B**) Dimension 2: Silver-stained 15% denaturing gel separating proteins in the single-band excised from the nondenaturing gel. (**C**) ATPase activity of detergent solubilized F_oF_1 (◯) and n-F_oF_1 (□) versus time at 25°C normalized to the initial activity of 110 and 145 s^{-1}, respectively.

Nanorods observed in Figure 2B were specifically bound to the c-ring of F_oF_1 on the microscope slide as n-F_oF_1 that lacked the c2∇C mutation failed to bind nanorods (Figure 2C). The stability of ATPase activity of the n-F_oF_1 complex (Figure 1C) is important due to the time required to complete single-molecule experiments. The abundance of n-F_oF_1 observed to rotate was at least 25% of the molecules in an average field of view that typically contained about 250 molecules (Figure 2B), which was comparable to the abundance observed using purified F_1-ATPase (York *et al*, 2007).

High-speed rotational power stroke measurement using gold nanorods

As shown in Figure 3, gold nanorod rotation results in a change in the intensity of red light scattered from the nanorod when viewed through a polarizing filter (Sönnichsen and Alivisatos, 2005; Spetzler *et al*, 2006). The intensity of red scattered light from a nanorod changes in a sinusoidal manner as a function of the rotary position of the nanorod relative to the plane of polarization with minimal and maximal intensities separated by 90° (Spetzler *et al*, 2006). Figure 3B shows the distribution of scattered red light intensities from a single-nanorod immobilized to the surface of a microscope slide as a function of the rotational position of the polarizing filter. At each position of the polarizer, the scattered light intensity was sampled 3520 times under conditions comparable to that used to measure rotation of n-F_oF_1 molecules. The sample number of 3520 was used because it corresponds to the average number of rotational power stroke

Table I Biochemical characterization of F_oF_1 mutants that lack transient dwells

Strain	k_{cat} ATPase (s^{-1})	k_{cat} ATPase + DCCD (s^{-1})	ATPase in SBP μmol ATP min^{-1} mg $protein^{-1}$	ATPase-dependent proton pumping (% of WT)
n-F_oF_1 (WT)	140	21	1.8	100
n-F_oF_1-cD62G[a]	130	130	0.8	0
n-F_oF_1-aR210G	20	20	1.1	0
n-F_oF_1-a∇14	90	90	0.4	0

[a]cD62 is so named due to the c2∇C insert mutant used for biotinylation.

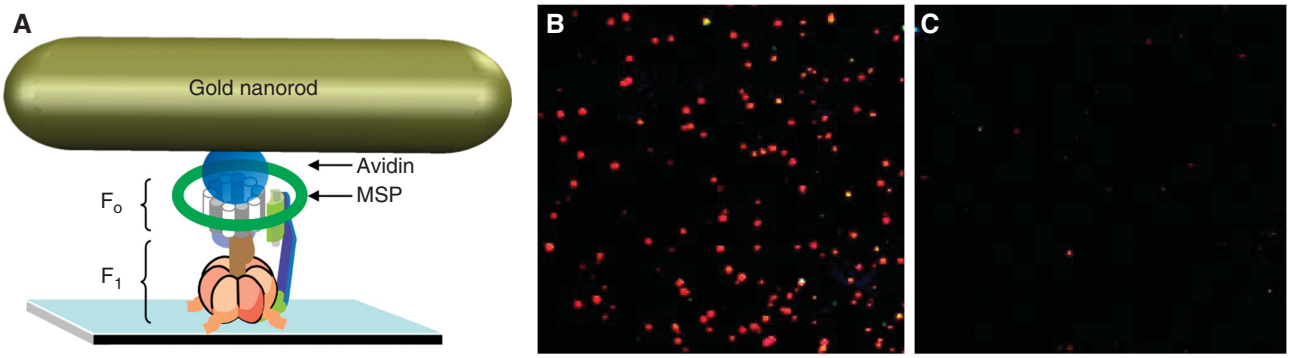

Figure 2 F_oF_1 nanodiscs (n-F_oF_1) in single-molecule rotation studies. (**A**) Microscope slide bound n-F_oF_1 attached via β-subunit N-terminus 6 × His tags attached to an avidin-coated 77 × 39 nm^2 nanorod via a biotinylated subunit-c cys. (**B**, **C**) Microscope fields-of-view of gold nanorods (red and green dots) bound to a slide coated with n-F_oF_1 in which subunit-c contained (**B**) or lacked (**C**) the cys insertion mutation.

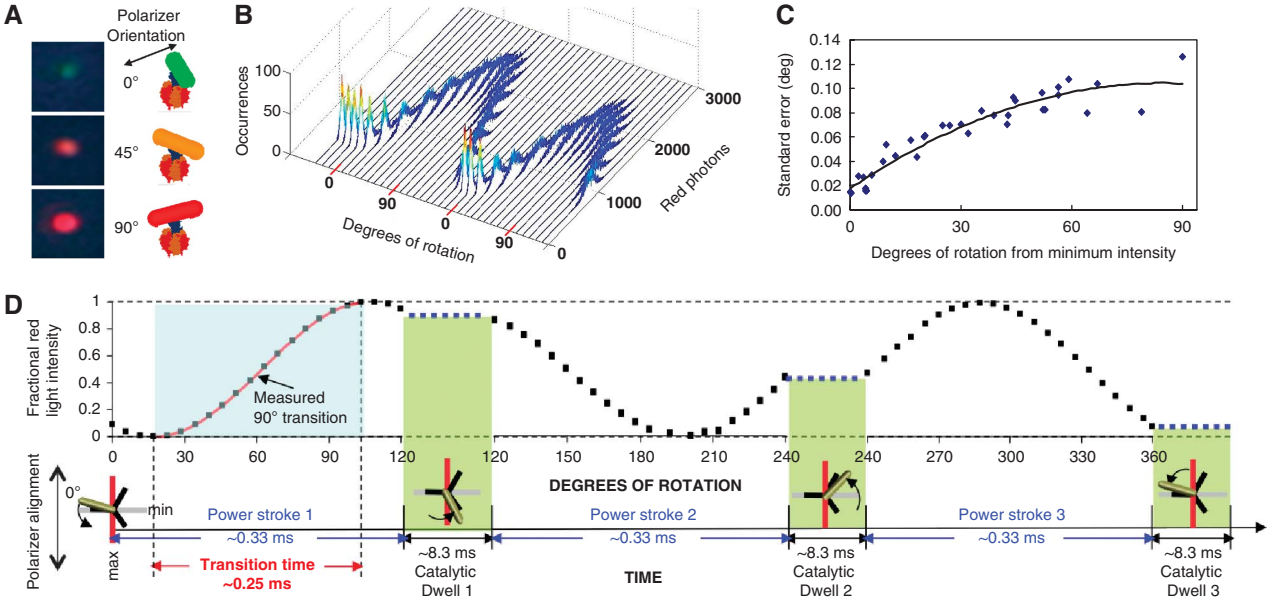

Figure 3 Use of nanorods to measure c-ring rotation of n-F_oF_1. (**A**) Micrographs of white light scattered from a single-gold nanorod viewed through a polarizing filter, and as a schematic showing the orientation of the nanorod to the polarizer. Measurement of rotation position is made only with the intensity of polarized red light scattered from the nanorod. (**B**) Histograms of the intensity of red light scattered from a single nonrotating nanorod fixed to a slide as a function of the rotational position of the polarizer. Each histogram contains 3520 measurements at each position of the polarizer obtained with the data acquisition speeds used to collect data points for c-ring rotation. The polarizer was then rotated counterclockwise by 10°, and data collection was repeated. (**C**) Standard error of nanorod rotational position versus degrees of rotation of the polarizer from the minimum intensity of light scattered from the nanorod as determined by Equation (1). (**D**) Relationship between a 120° power stroke and a 90° measured rotational transition. Theoretical plot of the intensity of scattered red light from a nanorod during one complete revolution that involves three consecutive power strokes and three consecutive catalytic dwells separated by exactly 120°. The nanorod is initially positioned almost, but not exactly perpendicular to the orientation of the polarizer such that the scattered light intensity goes through a minimum then a maximum prior to catalytic dwell 1. A transition includes the data between the minimum and maximum intensities representing 90° of the 120° of rotation for analysis. When initial alignment of the nanorod is exactly at the minimum and each of the successive power strokes is exactly 120°, the algorithm selects transitions for power strokes 1 (min to max) and 3 (max to min).

events measured for each n-F_oF_1 molecule during the 50-s data acquisition period used for all measurements reported here.

The scattered light intensity from the nanorod in Figure 3B varied between maximum and minimum values of 2500 and 500. The difference between these values resulted in a dynamic range of about 2000 photons per sample, which determined the sensitivity of the measurement. This was the minimum dynamic range used to measure rotation (the average range was ~3000 photons per sample), and thus serves as the upper limit for determining the error in the measurement of rotational position. The error in the determination of rotational position primarily results from variations in the intensity of scattered photons from the nanorod. The distribution of light intensity scattered from the nanorod was narrower at polarizer angles in which the intensity was at a minimum than that observed at the maximum. The degrees of rotation during a transition were derived from the arcsine of the fractional intensity of light scattered from the nanorod by Equation 1:

$$\theta = (\text{asin}\, \text{I})180\pi^{-1} \quad (1)$$

where θ is degrees of rotation, and I is the fractional intensity of scattered light. Consequently, the standard error in the measurements of Figure 3B varied between about 0.02 and 0.12 degrees as the scattered light intensity varied between minimum and maximum values (Figure 3C).

A saturating concentration of 1 mM Mg^{2+}-ATP was used for all rotational measurements reported here. Under this condition, F_1-ATPase-dependent power strokes occur in uninterrupted 120° rotational events separated by 8.3 ms catalytic dwells (Spetzler *et al*, 2006). A schematic of scattered light intensity during three consecutive power strokes (one complete revolution) is shown in Figure 3D when the nanorod was initially aligned nearly, but not exactly, perpendicular to the polarizer. As the stochastic nature of the enzyme results in a variation in the rotational position of each catalytic dwell (Yasuda *et al*, 2001), the alignment of the nanorod with the polarizer will show small variations during the data collection period. Consequently, the most sensitive and precise measure of rotational position during a power stroke is obtained when the nanorod rotates through the parallel and perpendicular alignment of the polarizer during a single 120° power stroke. This was measured as a change between maximum and minimum intensities of the scattered light, which corresponds to 90° of rotation, and an algorithm was used to collect these data as described previously (Spetzler *et al*, 2006).

The time required for 90° of continuous rotation to occur is defined as the transition time (Figure 3D). If the nanorod is initially aligned perpendicular to the polarizer and the three consecutive power strokes are exactly 120° during a single revolution such that the nanorod is also perpendicular during catalytic dwell 3, the algorithm will analyse transitions from power strokes one and three. In practice, the number of consecutive power strokes analysed is randomized by the stochastic nature of the molecular motor. Due to the randomization, there is an equal probability that the 90° increments of rotation measured as transitions represents the beginning, the middle, and the end of each 120° power stroke such that the entire power stroke is sampled in the course of the ~3520 power stroke events monitored for each molecule during the 50-s of data acquisition.

Appearance of transient dwells independent of proton translocation

In single-molecule studies of 320 n-F_oF_1 molecules (~3520 transitions molecule^{-1}), we observed two populations of n-F_oF_1 molecules based on differences in the transitions (Figure 4A, open and solid black squares) acquired during the 50-s of rotation measured for each molecule. The transitions in one population appeared nearly identical to those observed with isolated F_1-ATPase-driven rotation (circles). These transitions were similar in that the power strokes of both rotated continuously for the full 90° of the transition and achieved equivalent velocities. The other population of n-F_oF_1 molecules took much longer to complete a 90° transition due to the appearance of transient dwells. The transient dwells were present in >90% of the power strokes of any n-F_oF_1 molecule in this latter population, whereas <1% of the F_1 power strokes had anomalies that appeared similar to

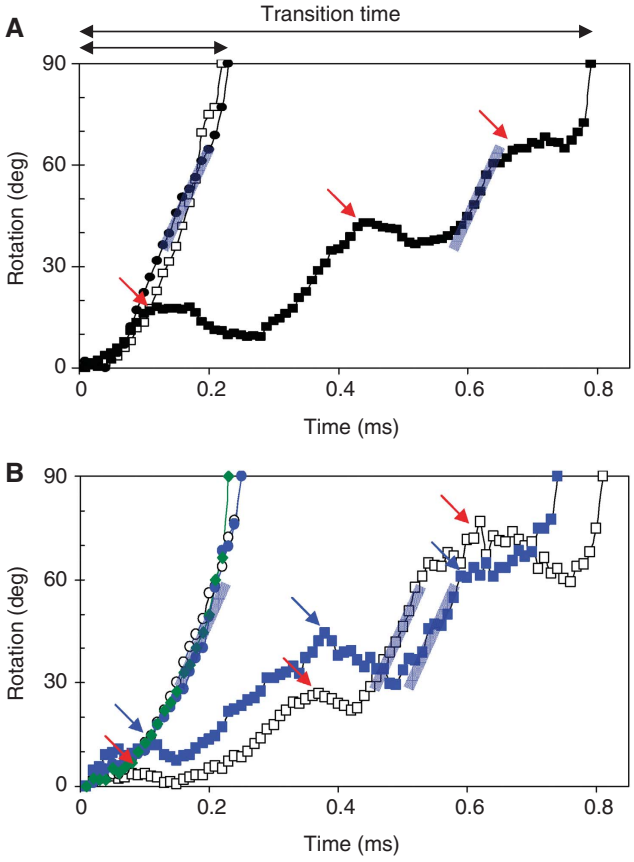

Figure 4 Power stroke events with and without transient dwells due to ATPase-driven rotation of single molecules. Arrows indicate transient dwells. (**A**) Example transitions for F_1 (●), as well as for n-F_oF_1 with (■) and without (□) transient dwells. (**B**) Transitions obtained from n-F_oF_1-aV14 (◆), n-F_oF_1-aR210G with (□) and without (○) transient dwells, and n-F_oF_1-cD62G with (■) and without (●) transient dwells. Nanorod attachment occurred via the γ-subunit for F_1 or via the c-ring for n-F_oF_1. Data were acquired at 100kHz in the presence of 15% PEG400 (v/v) and 1 mM MgATP, and were converted from scattered light intensity to degrees of rotation by equation (1). Grey lines indicating the power stroke velocity have the same slope.

Table II Periodicity of transient dwells observed during rotational transitions in the presence of 15 and 30% PEG400

Strain	Rotation between transient dwells	Transient dwells per 90° rotation	Molecules examined	Transitions examined
WT	37° ± 0.5	2.48 ± 0.043	45	36 421
cD62G	38° ± 0.8	2.45 ± 0.065	17	11 458
aR210G	37° ± 0.5	2.50 ± 0.039	17	5856

these dwells. The power stroke velocity was not significantly altered by the presence of transient dwells as indicated by the blue lines in Figure 4 that have the same slopes.

During the transient dwells, the c-ring often rotates a few degrees in the reverse direction (Figure 4). An average interval of 37.3° ± 0.75 between transient dwells in a transition was observed (Table II) as derived from Equation (1). The 90° transitions were also found to contain an average of ~2.5 transient dwells. Both of these measurements translate into an average of ~10 transient dwells for each complete revolution of the c-ring, indicating that the transient dwells result from an interaction between subunit-a and each c-subunit in the 10 c-subunit *E. coli* ring (i.e. every 36°). These data also show that the occurrence of longer rotational stepping that skip one or more c-subunits is rare.

To determine whether the appearance of transient dwells resulted from the aR210–cD61 interaction essential to F_o proton translocation, we studied the mutants n-F_oF_1-aR210G and n-F_oF_1-cD62G (instead of cD61 due to the c2∇C insertion) that lack these charged groups. Transitions from molecules of both mutants contained transient dwells (Figure 4B) that had the same periodicity and duration of those lacking these mutations (Table II). This indicates that the transient dwells do not result from the periodic cD61–aR210 interaction.

The transient dwells were eliminated by a mutation to subunit-a (a∇14) as shown in Figure 4A. All 219 n-F_oF_1-a∇14 molecules examined had continuous power strokes that lacked transient dwells, and were comparable to those of F_1. The subunit-a mutation designated n-F_oF_1-a∇14 was formed by site-directed mutagenesis during PCR at suboptimal conditions when making the aR210G mutant (see Materials and methods), and was identified by sequencing. This mutant has a 14 amino acid insert that duplicates the sequence in transmembrane helix-4 (TMH4) between residues 204 and 217, except that aR210 has been converted to valine and glycine in the repeated sequences (Figure 5A). The mutation did not alter the subunit composition of F_oF_1 as determined by PAGE (Figure 5B). However, subunit-a in F_oF_1-a∇14 appears to run as a slightly higher molecular weight band. The F_oF_1-a∇14 had a k_{cat} of 90 s^{-1} for ATPase activity that was not susceptible to inhibition by DCCD (Table I), and membranes containing this mutant were unable to catalyse ATPase-dependent proton translocation. These results are similar to those obtained for other aR210 mutations (Lightowlers *et al*, 1987; Ishmukhametov *et al*, 2008).

The data in Figures 4 and 5 indicate that the transient dwells result from a periodic interaction between subunits-a and c in F_o that has not been previously described. Figure 5C uses the well-established subunit-a folding pattern (Zhang and Vik, 2003b; Moore and Fillingame, 2008) to show the approximate locations of the residues affected by the a∇14 mutation. Due to the restraints imposed by TMH3 and TMH5, the hydrophobic insert likely extends TMH4 to displace helix 4C and to a smaller extent helix 3C. In the crystal structure of the chloroplast F_oF_1 c-ring (Figure 5D), residues analogous to *E. coli* cD44 and cR50 form a ring of charged residues (Vollmar *et al*, 2009) that is also evident in the c-ring structures from *Ilyobacter tartaricus* (Meier *et al*, 2009; Pogoryelov *et al*, 2009) and *Saccharomyces cerevisiae* (Dautant *et al*, 2010). Other than aR210 and cD61, the interface between helices 3C and 4C and the cytoplasmic side of the c-ring is the only location where conserved charged residues capable of forming salt bridges are juxtaposed.

Effects of nanodiscs and F_o mutations on Torque

Figure 6 shows transition times as a function of PEG400 concentration, which was used to increase the viscosity of the solution as a means to impose a greater load on the motor. PEG400 molecules were chosen because they were determined to behave as a Newtonian fluid (Hornung *et al*, 2008). As such, they are too small to be pulled along by the rotating nanorod, and thus do not make secondary nonlinear contributions to the drag. The increased drag on the gold nanorod due to the viscosity of the PEG400 solution exerts a load on the motor that slows the power stroke velocity, which can be used to determine the torque (Hornung *et al*, 2008). For a given size of nanorod, the angular velocity is determined by the rotational distance (arc distance) divided by time. In the absence of the transient dwell, the average angular velocity is calculated using the arc distance of the rod moving 90° divided by the transition time. In the presence of the transient dwell, the average angular velocity is the arc distance of the rod moving 36° divided by the average time between transient dwells.

Torque was calculated from the drag and the velocity by Equation (2):

$$T = \Gamma w, \tag{2}$$

where Γ is the drag force and ω is the angular velocity of the power stroke. The dependence of the purified F_1-ATPase power stroke velocity on the PEG400 concentration was about the same as that of n-F_oF_1, and was not significantly altered by any of the mutations examined (Figure 6), resulting in ~62 pN nm of torque. This value is closely similar to that reported previously for purified *E. coli* F_1-ATPase (Hornung *et al*, 2008). Thus, incorporation of F_oF_1 into nanodiscs did not significantly alter the abundance of molecules observed to rotate, or the power stroke velocity (i.e. the torque). Nanodiscs also increased the stability of the ATPase activity of the enzyme. Based on these results, we conclude that incorporation of the F_o into nanodiscs does not influence the speed or efficiency of the rotor.

Transient dwells form when viscous drag slows rotation below a threshold speed

The proportion of F_oF_1 molecules that exhibited transient dwells increased with the viscosity of the medium (Figure 7A). All molecules measured at PEG400 concentrations below 15% had the same rotational profile of power stroke transitions as that of F_1. The abundance of molecules with transient dwells increased from 27 to >80% for PEG400

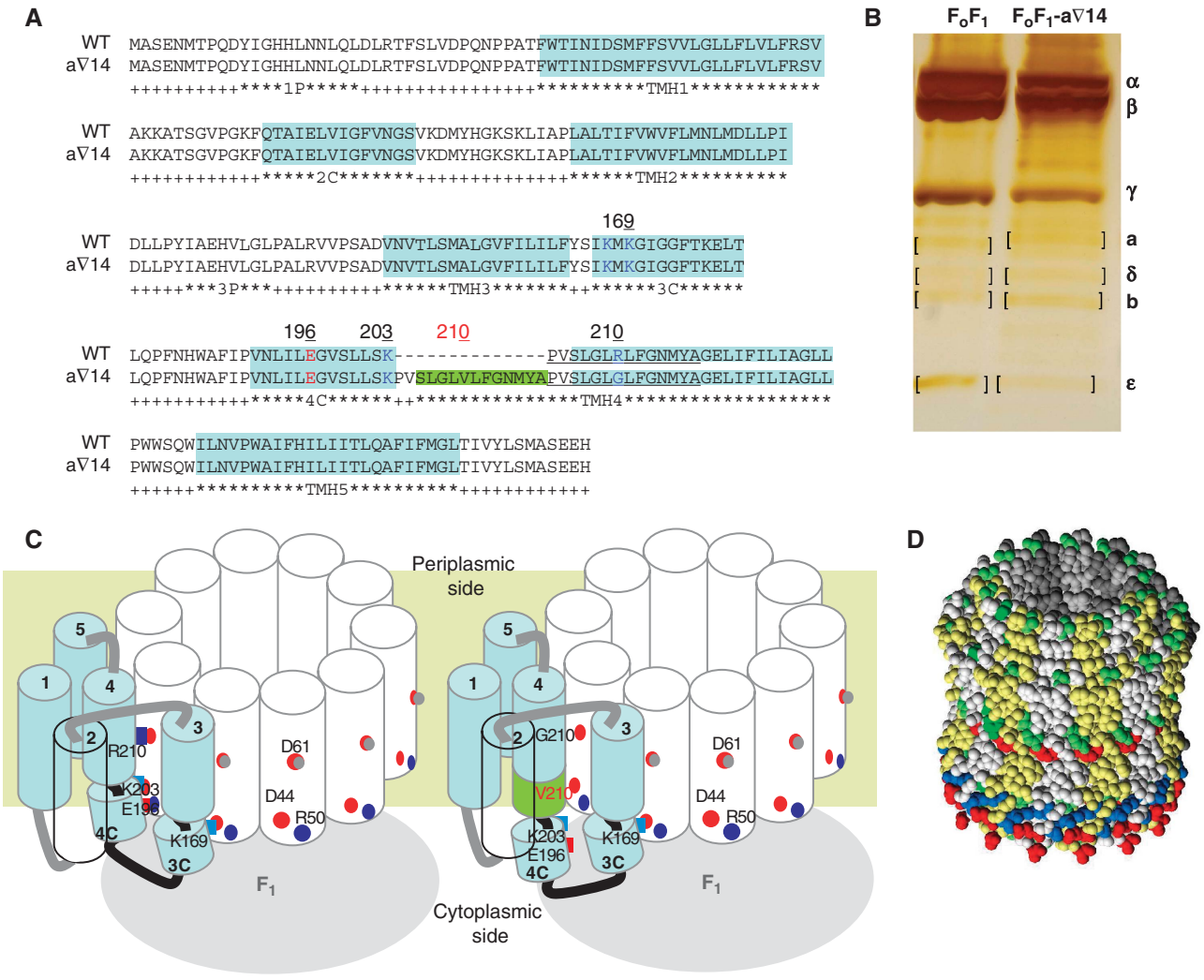

Figure 5 Interaction between subunits a and c. (**A**) Subunit-a amino acid sequences of F_oF_1 and F_oF_1-aV14 showing the helical regions (blue) as established by Zhang and Vik (2003b); and Moore and Fillingame (2008). In the n-F_oF_1-aV14 mutant, a 14 amino acid sequence was duplicated (green bar and underlined) that included arginine at position 210, which was replaced by valine and by glycine in the duplicated region. (**B**) Silver-stained 8–16% gradient gel (Bio-Rad) of F_oF_1 and F_oF_1-aV14 subunits separated by SDS–PAGE. (**C**) Folding of the subunit-a transmembrane helices (TMH) in the membrane relative to the position of residues cD44, cR50, and cD61 in the c-ring as established by Zhang and Vik (2003b); and Moore and Fillingame (2008). (**D**) C-ring crystal structure from chloroplast F_oF_1 (Vollmar *et al*, 2009). Hydrophobic residues (yellow, grey) distinguish c-subunits, whereas polar, positive, and negative residues are green, blue, and red.

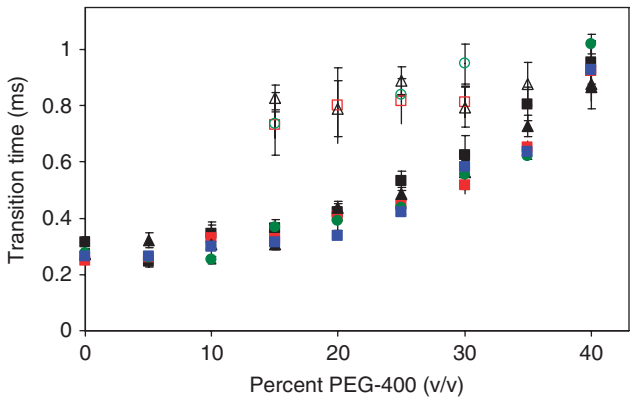

Figure 6 Transition times of rotational power strokes as a function of PEG400 concentration. Average transition times with (open symbols) and without (closed symbols) transient dwells for n-F_oF_1 (Δ, ▲), n-F_oF_1-aR210G (□, ■), n-F_oF_1-cD62G (○, ●), n-F_oF_1-aV14 (■), and F_1 (■) at each concentration of PEG400. Approximately 3520 transitions were acquired for analysis from each molecule examined.

concentrations between 15 and 35%. A similar trend was observed with n-F_oF_1-aR210G and n-F_oF_1-cD62G molecules as a function of PEG400 concentration although the total abundance was somewhat lower than that observed with n-F_oF_1.

The average transient dwell duration was ~200 μs at 15% PEG400, but decreased with increasing PEG400 (Figure 7B). This was determined by the difference in the average transition times with and without transient dwells divided by the average number of transient dwells per transition (Figure 6), and was confirmed by direct measurement of the duration of about 200 transient dwells at each PEG400 concentration. It is noteworthy that the decreases in transient dwell duration were compensated by slower power stroke velocities at higher PEG400 concentrations (Figure 7C). Consequently, for those molecules that exhibited transient dwells, the total transition time did not change as a function of PEG400 (Figure 6). At 40% PEG400, the power stroke velocity was too slow to distinguish changes in the slope that identify the existence of transient dwells. The same relationship between

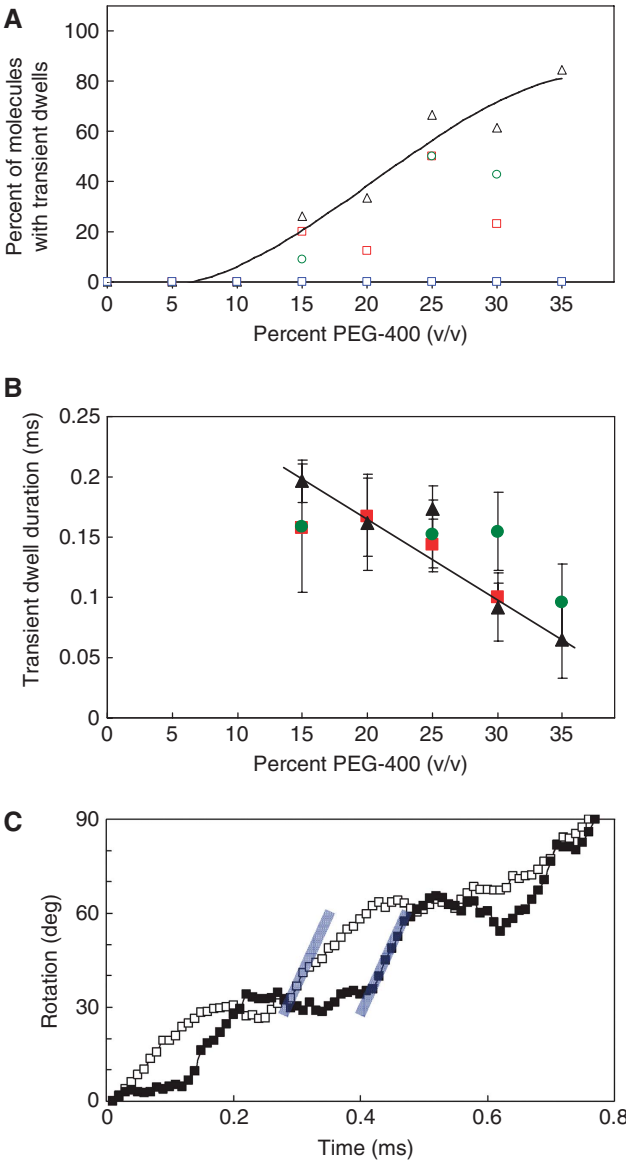

Figure 7 Effects of viscosity on the appearance and duration of transient dwells. (**A**) Abundance of n-F_oF_1 (Δ), n-F_oF_1-aR210G (□), F_oF_1-cD62G (○), and n-F_oF_1-a∇14 (□) molecules with transient dwells as a function of PEG400 concentration. (**B**) Transient dwell duration of n-F_oF_1 (▲), n-F_oF_1-aR210G (■), and n-F_oF_1-cD62G (●) as a function of PEG400. (**C**) Transitions with transient dwells at 15% PEG400 (■) and 30% PEG400 (□) have the same transition time, but different transient dwell durations. Grey lines indicating the power stroke velocity in the presence of 15% PEG400 have the same slope.

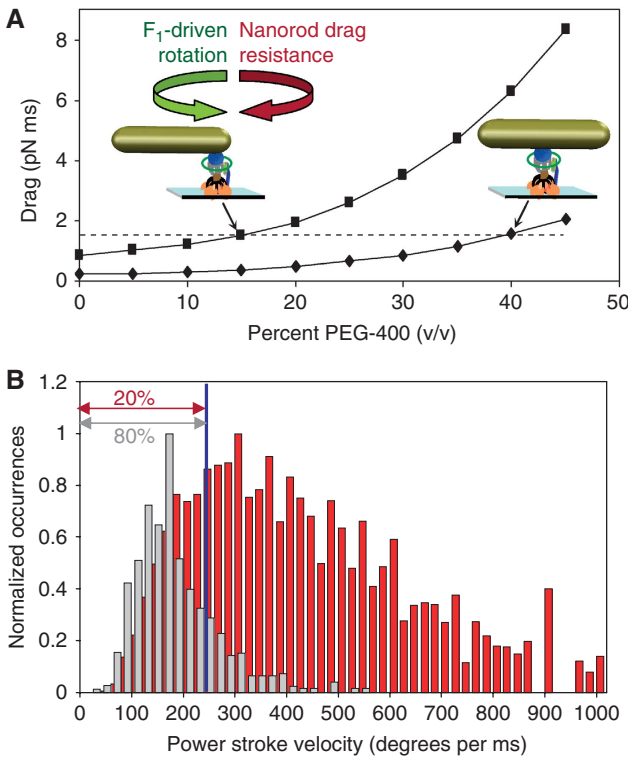

Figure 8 Requirements for transient dwell formation. (**A**) Minimum and maximum drag imposed by a $77 \times 39\,nm^2$ gold nanorod on the motor as a function of PEG400 based upon c-ring attachment in the middle (◆) or the end (■) of the nanorod as determined by Equation (2). Dotted line: threshold of drag for the appearance of transient dwells in Figure 4A. (**B**) Distributions of power stroke velocities from single molecules with $77 \times 39\,nm^2$ nanorods at 15% (red) and 35% (grey) PEG400. Velocity at blue line is $220^\circ\,ms^{-1}$. The slowest 20 and 80% transitions at 15 and 35% PEG400 is indicated.

transient dwell duration and transition time was also observed with the n-F_oF_1-aR210G and n-F_oF_1-cD62G mutants.

The appearance of transient dwells is not an effect of the binding of PEG400 to the enzyme as none of the n-F_oF_1-a∇14 molecules contained these dwells regardless of the PEG400 concentration. Alternatively, the transient dwells may appear when PEG400 increases the viscous drag on the motor beyond a threshold value. To test this hypothesis, the maximum and minimum drag generated by a $77 \times 39\,nm^2$ gold nanorod was calculated as a function of PEG400 concentration when the axis of rotation was at the end or in the middle of the nanorod, respectively (Figure 8A). Comparison of direct measurements of the drag on the nanorod (Hornung *et al*, 2008) showed that the propeller model provided a close approximation of the drag force as a function of PEG400 concentration. Based on this model, the drag force is approximated by equation (3),

$$\Gamma = \frac{4\pi\mu(L_1^3 + L_2^3)}{3\cosh^{-1}(h/r)}, \qquad (3)$$

where L_1 and L_2 are the length of the propeller extending from the rotational axis, r is the radius of the rod, μ is the viscosity of the medium, and h is the height of the cylinder axis relative to the surface. Using Equation (3), the load exceeds ~1.4 pN ms for the subset of molecules in which the c-ring is attached to the end of the nanorod when transient dwells first become apparent (15% PEG400). This same load on the motor occurs at 40% PEG400 when the rotation axis is in the middle of the nanorod. This suggests that the appearance of transient dwells occurs when the load on any n-F_oF_1 molecule exceeds the threshold of 1.4 pN ms. As the binding position of the c-ring along the length of the nanorod is random, the percentage of molecules that exceed this threshold increases as a function of PEG400, consistent with the trend observed in Figure 7A. Moreover, when the transient dwell is present for a particular molecule, it is evident in every observed transition, suggesting that the cause of the transient dwell is constant for any given

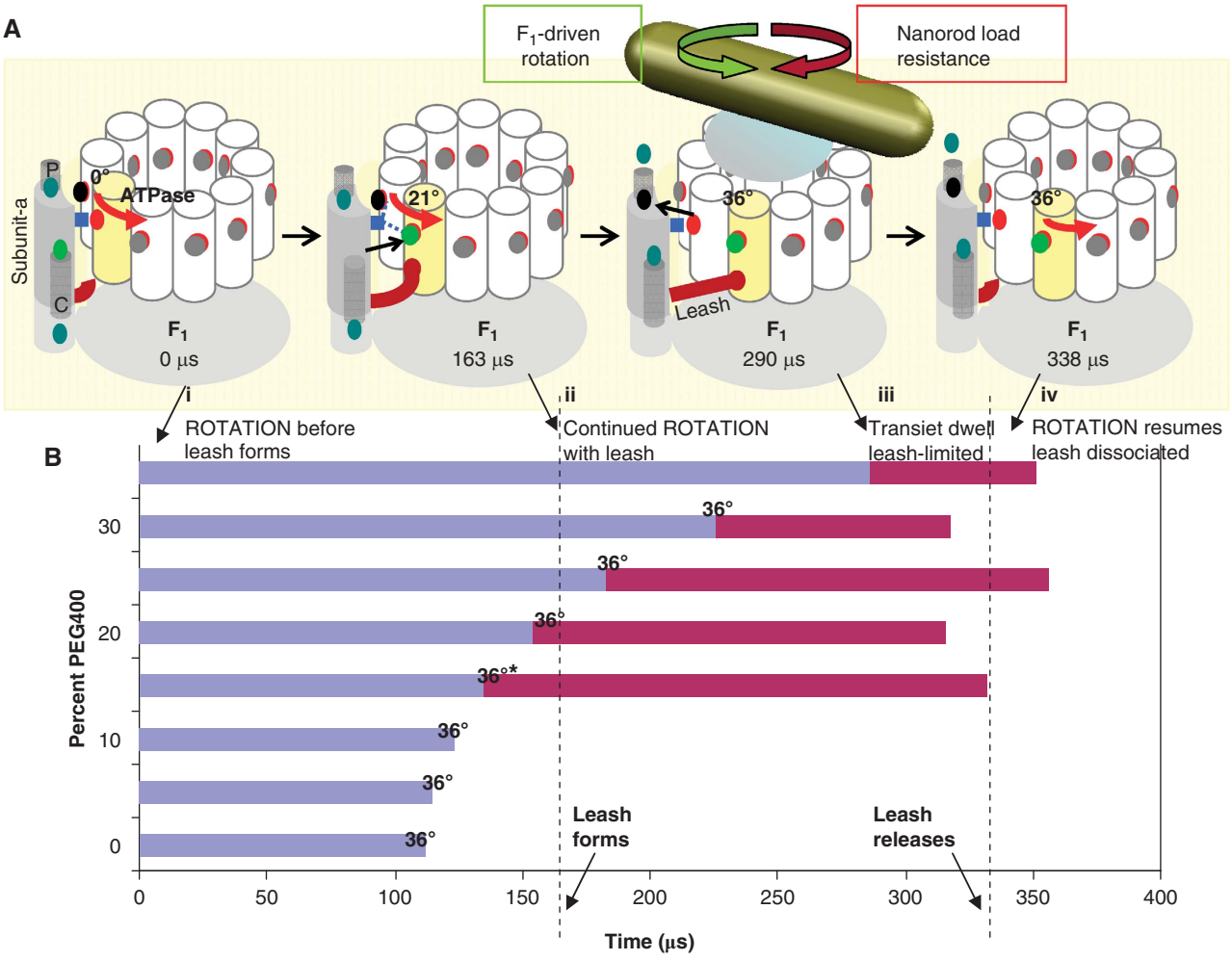

Figure 9 Timing of formation and release of the leash interaction relative to c-ring rotation. (**A**) Model of leash interaction between subunits a and c at 35% PEG400. Green dots: H^+ in subunit-a cytoplasmic (C) and periplasmic (P) half-channels. Grey/black dots: H^+ on cD61 (red dots). Periplasmic half-channel in subunit-a (P). (i) Rotation without leash; (ii) Leash forms, but rotation continues; (iii) Rotation at end of leash; (iv) Leash dissociates, rotation resumes. (**B**) Time course of c-ring rotation and transient dwell duration as a function of PEG400 concentration. Blue bars indicate average time for the c-ring to rotate 36°. At 15% PEG400, the subpopulation of molecules that gave rise to the transient dwells rotated more slowly (36°*) than the average rotational velocity (Figure 8B). Red bars indicate average transient dwell duration.

molecule, as is the case for the binding orientation of the rod to the motor.

The distributions of power stroke velocities observed in the presence of 15 (red bars) and 35% (grey bars) PEG400 is shown in Figure 8B, where the fraction of molecules that exhibit transient dwells was 20 and 80%, respectively. Thus, the molecules subject to the drag on the motor exceeding the 1.4 pN ms threshold will have power stroke velocities in the slowest 20 and 80% of the two distributions at these PEG400 concentrations. This corresponds to molecules with velocities $<220^\circ\,ms^{-1}$ (blue line) for both distributions. At this velocity, the c-ring rotates 36° in about 163 μs. As the interaction responsible for the transient dwells occurs about every 36° (i.e. between subunit-a and each c-subunit, Table II), the time constant for formation of the transient interaction is ~160 μs. Thus, the drag threshold needed to observe transient dwells is actually the extent to which the power stroke velocity must be decreased in order to allow the interaction to form within the time that the c-ring rotates 36°. Any molecule that rotates 36° in <163 μs does not exhibit transient dwells.

The interaction responsible for the transient dwell behaves as a leash

Figure 9 shows the average time courses of n-F_oF_1 molecules as a function of PEG400 concentration. Blue bars represent the average time required for the c-ring to rotate 36° based on distributions like those in Figure 8B, and red bars show the average transient dwell duration (Figure 7B). The rotational velocity of all the molecules in 0–10% PEG400 was too fast for the transient interaction to form. At 15% PEG400, the 20% of molecules subject to a load sufficient to allow the transient interaction to form (indicated as 36°*) had a velocity less than the average of the distribution (Figure 8B). For all the molecules exhibiting transient dwells regardless of PEG400 concentration, the average total time required to rotate 36° and complete the transient dwell was 338 μs independent of the power stroke velocity. As the time constant to form the subunit a–c transient interaction is 163 μs, these results indicate that the time constant for the termination of the interaction is ~175 μs, independent of PEG400 concentrations. The turnover time of the

interaction responsible for the transient dwells is then ~338 μs.

The extent to which the c-ring has rotated after 163 μs (transient interaction formation time) decreases as the rotational velocity is slowed by increased load on the motor. For example, at 25 and 35% PEG400, the interaction forms after the c-ring has rotated ~31 and 21°, respectively (Figure 9A). As transient dwells appear about every 36°, the decrease in observed transient dwell duration (161 and 59 μs at 25 and 35% PEG400, respectively) indicates that formation of the transient interaction acts as a leash. At the slowest velocities in the distribution of any given molecule (e.g. Figure 8B), the transient interaction forms after the c-ring has rotated only a few degrees such that the leash must allow rotation to continue to a limit of ~36°.

Discussion

Model for the leash mechanism

A schematic of F_oF_1 illustrating the steps in the F_o leash mechanism is summarized in Figure 9A for F_1-ATPase-driven rotation in 35% PEG400 based on the data presented here. In this model, all cD61 carboxyl groups (red) dots are protonated (grey/black dots) except in the yellow c-subunit where cD61 interacts with aR210 (blue square). (i) At the start of an F_1-ATPase 120° power stroke, constant torque is applied to the c-ring, which begins to rotate in the absence of the leash. Residue cD61 of the yellow c-subunit becomes protonated (green dot) from the cytoplasmic half-channel (C) as it rotates away from aR210. (ii) Formation of the transient leash occurs at ~163 μs, at which point the c-ring has rotated 21°, which does not interfere with rotation. (iii) Rotation is interrupted at 290 μs when the leash becomes fully extended upon rotation of the c-ring by 36°, at which point the transient dwell becomes apparent. A proton (black dot) moves to the periplasmic half-channel (P) as aR210 deprotonates cD61 on the adjacent c-subunit. (iv) Rotation resumes at 338 μs upon dissociation of the leash.

As the *E. coli* F_1-ATPase generates 62 pN nm of torque (Hornung *et al*, 2008), the leash is likely comprised of multiple salt bridges between subunit-a and the c-ring to be of sufficient strength to cause the transient dwells. With the exception of aR210 and cD61, conserved charged residues on both subunit-a and the c-ring that could participate in such intersubunit salt bridges occur only on the cytoplasmic side of the membrane (Figure 5). At this location, available crystal structures of c-rings (Meier *et al*, 2009; Pogoryelov *et al*, 2009; Vollmar *et al*, 2009; Dautant *et al*, 2010) all show a band of charged residues analogous to cD44 and cR50 in *E. coli*. Cross-linking studies between subunits-a and c support the juxtaposition of aE196 and cR50 (Jiang and Fillingame, 1998; Zhang and Vik, 2003a, b), and aqueous accessibility studies position aK169, aK203, aE196, and cR50 close to the cytoplasmic surface of the membrane facing subunit-a (Fillingame *et al*, 2000; Zhang and Vik, 2003b; Steed and Fillingame, 2009). This suggests that the axis of subunit-a, helix 4C may be more parallel to the membrane surface than is represented in Figure 5C. At this location, the deprotonated aE196 and cD44 carboxyl groups that could participate in salt bridges between subunits-a and c are not subjected to the large free energy penalty that would result if they were buried in the hydrophobic core of the membrane-like cD61 (Elston *et al*, 1998). Thus, the formation/dissociation kinetics of salt bridges formed from these groups is anticipated to be consistent with the transient dwells observed here.

Site-directed mutations that altered the charge of aE196 were found to significantly alter *E. coli* F_o-dependent proton translocation (Vik *et al*, 1988), and aE196 has been identified as one of three sites leading to oligomycin resistance in mitochondria (Breen *et al*, 1986; John and Nagley, 1986; Ray *et al*, 1988). Mutational studies have implicated that aE196 (Zhang and Vik, 2003a; Moore *et al*, 2008) and aK203 (Moore *et al*, 2008) participate in the proton half-channel between cD61 and the cytoplasm. Mutations aK203C (Angevine *et al*, 2007), aK167Q, and/or aK169Q (Lightowlers *et al*, 1987) do not effect the activity of F_oF_1 significantly. However, in each case, polar groups were created by these mutations, which would not eliminate the ability to form hydrogen bonds between subunits-a and c. It is noteworthy that participation in a proton half-channel and in the formation of the transient dwells observed here need not be mutually exclusive functions of a particular residue. These functions could be linked under conditions where the free energy from the PMF and the logQ are close to equilibrium. The results of the F_oF_1-a∇14 mutant reported here (Figure 4B) that eliminate the transient dwells are consistent with the juxtaposition of these residues on subunits-a and c. However, given that this mutant includes a 14 amino acid insertion, more experiments are required to pinpoint the specific interaction responsible for the transient dwells.

The results presented here support a mechanism for c-ring rotation when the F_1 motor is subjected to a load (Figure 9A). Under these conditions, the cycle of Figure 9A repeats with each c-subunit in 36° increments until the F_1-ATPase power stroke completes 120° to begin the next catalytic dwell (Figure 10A). This conclusion is supported by the observations of 2.5 transient dwells per transition with an average of 37° between transient dwells within a transition (Table II). These data suggest that double, triple, or multiple steps between transient dwells are rare. This means that on average, each 120° power stroke includes rotation of the c-ring by three complete c-subunit steps (36° each) and 12° of a fourth step. This partial fourth step can be accommodated by the observation presented here that the leash can form before the c-subunit has rotated the full 36°. The well-established compliance of the γ-subunit drive shaft (Sielaff *et al*, 2008) and the stochastic nature of F_1-ATPase-driven rotation (Yasuda *et al*, 1998) will also mediate the stoichiometric differences between F_o and F_1.

The lack of an effect of aR210G and cD62G mutations on the transient dwells reported here demonstrates that proton translocation is independent of, and not rate limiting to, the interactions responsible for the transient dwells during ATPase-driven rotation. Thus, even though the power stroke velocity at ⩽10% PEG400 occurs too quickly for the transient dwell to form (Figure 7A), ATPase-driven proton translocation across the lipid bilayer of the nanodisc can still occur (Figure 10B). This conclusion is consistent with the much higher rates of F_o-dependent proton translocation that can occur in response to a PMF after F_1 has been removed (Franklin *et al*, 2004; Wiedenmann *et al*, 2008), and the fact that the proton translocation rate of F_o does not saturate at high-driving force (Feniouk and Junge, 2008). Based on the leash formation rate of 163 μs/H^+ reported here, the leash

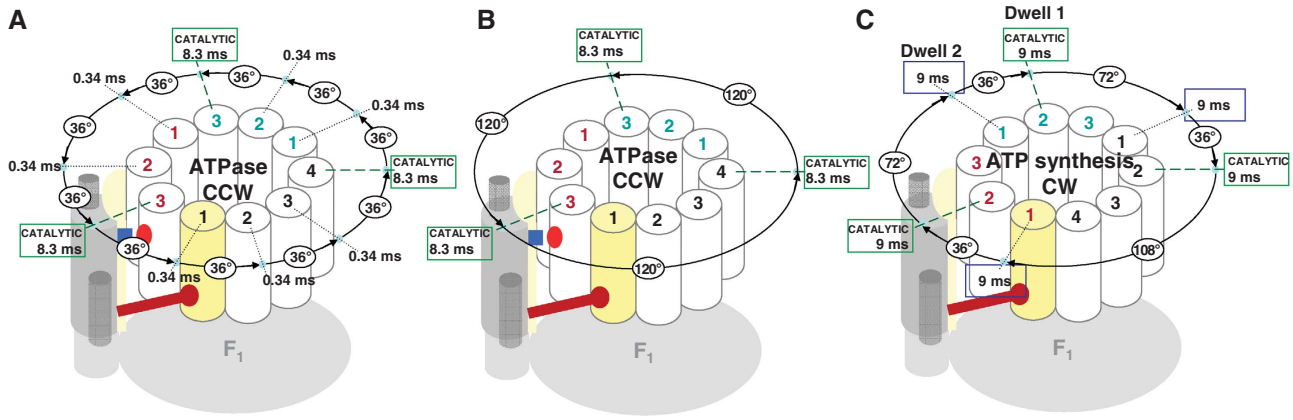

Figure 10 Summary of F_oF_1 rotational stepping events powered by F_1 during ATP hydrolysis and by F_o during ATP synthesis. (**A**, **B**) F_oF_1 c-ring transient dwells during F_1-ATPase-driven rotation with 1 mM MgATP in the presence (**A**) and absence (**B**) of viscosity-induced load. The ATP-waiting dwells were not observed in the data presented here or by Düser *et al* (2009) due to the use of the saturating substrate concentrations. (**C**) Model for the grouping of F_oF_1 c-ring rotation events during ATP synthesis powered by F_o with a $\Delta pH = 4.1$ at saturating [ADP] and [Pi] consistent with (Düser *et al*, 2009).

will form until F_o proton translocation rates exceed 6135 H^+ s^{-1}. Chloroplast F_o was observed to exceed this rate, and a PMF could not be found that was large enough to maximize the proton translocation rate (Feniouk and Junge, 2008). However, direct comparison of chloroplast and *E. coli* F_o indicates that the latter translocates protons more slowly (Wiedenmann *et al*, 2008), such that leash engagement will occur in *E. coli* F_oF_1 even at the highest reported rates of 3100 H^+ s^{-1} (Franklin *et al*, 2004).

Although the highest reported ATP synthesis rates of 100 s^{-1} correspond to 3.3 ms/H^+, or ~10 ms per 120° (Senior *et al*, 2002), a significant amount of that time is consumed by the catalytic dwell. Düser *et al* (2009) reported 9 ms dwells during ATP synthesis with *E. coli* F_oF_1, which is consistent with the 8.3-ms catalytic dwell observed for *E. coli* F_1-ATPase (Spetzler *et al*, 2006). Due to the F_1 requirement of 120° steps for each catalytic dwell, the rotational stepping of the c-ring during ATP synthesis must also occur in approximate increments that sum to ~120°. As Düser *et al* (2009) observed that about 50% of the c-ring substeps were 36°, each 120° step is likely the sum of one 36° substep and one substep of a larger step size (Figure 10C). This corresponds to a 36° + 108° substep combination between catalytic dwells involving c-ring rotation by four c-subunits, and a 36° + 72° substep combination between the two catalytic dwells involving rotation by three c-subunits. This hypothesis predicts a 1:2 ratio for the 72° and 108° substeps, which is similar to the observed ratio of 1:3. This difference can be compensated by the stochastic nature of the enzyme, as evidenced by occasional (3%) 144° steps (Düser *et al*, 2009), and by compliance of the γ-subunit (Sielaff *et al*, 2008).

As 9 ms dwells were observed after each 36° substep and each multiple (double or triple) subunit-c step (Düser *et al*, 2009), the model of Figure 8C has two 9 ms dwells per each 120° of rotation that results in ATP synthesis. If transient dwells occur under these conditions as they are suggested to do by the overall proton translocation rate, then these dwells that result from the leash with a 335-μs turnover time likely occurred during the multiple subunit-c steps during ATP synthesis and were not resolved by the 2-ms time resolution of the FRET measurements. Although one of the two 9 ms dwells during ATP synthesis is likely the catalytic dwell, more work is required to understand the relationship between the 9-ms, 36° substep dwell observed during ATP synthesis and the much shorter 36° transient dwells that occur during ATP hydrolysis reported here.

Transient dwells occur under conditions common for ATP synthesis in vivo

The experiments presented here indicate that the leash forms when a load on the F_1-ATPase motor is sufficient to slow the rotational velocity below a threshold value to provide enough time for the interaction between subunits a and c to occur. *In vivo*, proton translocation driven by a transmembrane electrochemical gradient powers c-ring rotation in the opposite (CW) direction from that driven by ATP hydrolysis (Börsch *et al*, 2002). The rate of ATP synthesis only becomes significant above an electric potential threshold, which for *E. coli* F_oF_1, is ~40 mV (Kaim and Dimroth, 1998). However, this threshold is dependent on Q, the ATP/ADP · P_i chemical potential (Turina *et al*, 2003). Thus, a small transmembrane proton gradient will cause the F_o motor to apply a load on F_1-ATPase-driven rotation similar to that induced by the viscous drag of PEG400 reported here.

Conversely, F_1 imposes a load on the F_o motor during ATP synthesis that is dependent on the ATP/ADP · P_i chemical potential. Although ATP synthesis rates of 100 s^{-1} (3.3 ms per H^+) can be achieved upon addition of saturating concentrations of ADP and phosphate in the absence of ATP, at steady state the enzyme sustains a concentration of 3 mM ATP at a $\log Q \cong 0.1$ in *E. coli* cells (Senior *et al*, 2002). Under these conditions, when the energetics of the PMF and Q approach equilibrium, the rate of c-ring rotation will be sufficiently slow for the leash to form. In so doing, the leash would limit the backward (ATPase) rotation of the c-ring to ~36° at steady-state conditions when ATP concentration is high, and thereby minimize ATP hydrolysis events relative to synthesis.

Potential relationship of the leash to the Brownian ratchet mechanism

A model for the role of the leash in PMF-powered CW c-ring rotation during ATP synthesis is shown in Figure 11. The PMF is represented by the disproportionate H^+ abundance aligned

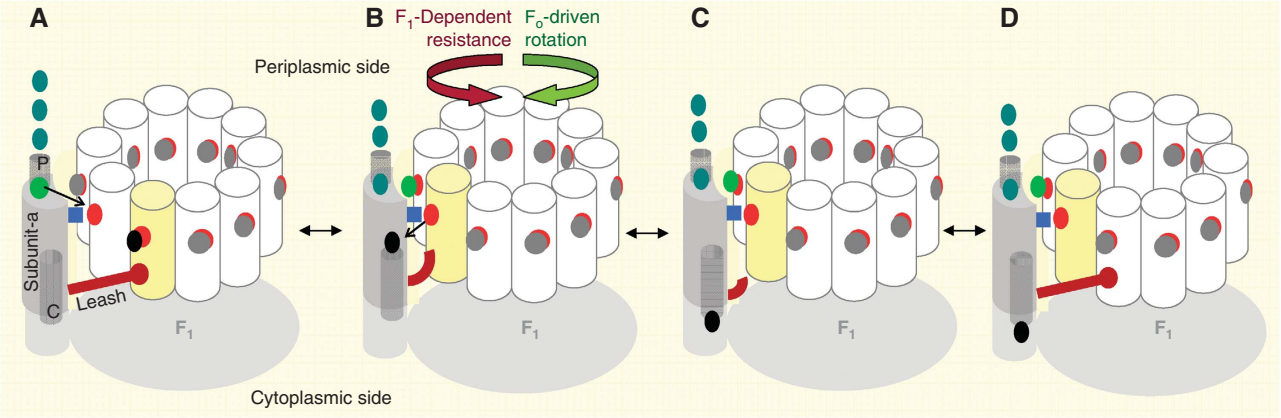

Figure 11 A model for a leash-based F_o ratchet mechanism during F_oF_1-ATP synthesis. (**A**) The end of the leash prevents further counter-clockwise rotation. Excess H^+ (green dots) on the periplasmic side indicates a PMF. (**B**) The leash limits Brownian-dependent back and forth c-ring motion to 36°. During clockwise rotation, subunit-a aR210 (blue square) displaces the H^+ (black dot) from yellow subunit-c cD61 (red dot) to the cytoplasmic half-channel (C), whereas the adjacent white subunit-c cD61 becomes protonated (light green dot) from the periplasmic half-channel (P). (**C**) The interaction responsible for the transient dwell dissociates. (**D**) Formation of the interaction at the end of the leash with the adjacent subunit-c ratchets the c-ring clockwise with H^+ translocation to power ATP synthesis.

with the half-channels (green dots). During the 36° of CW movement permitted by the leash (A→B), the c-ring accepts a proton from half-channel-P and donates a proton to half-channel-C, which is reversed by CCW rotation (B→A). Upon dissociation of the leash (C), the probability that the leash will reform with the adjacent c-subunit that ratchets the c-ring clockwise to catalyse ATP synthesis (C→D) versus reforming with the same c-subunit (C→B) depends on the relative probabilities of c-ring protonation by each half-channel due to the availability of H^+ at each half-channel at that moment. The PMF promotes a higher probability of CW rotation. At high steady-state ATP concentrations, we anticipate that several C→B→C cycles will occur before a successful C→D step takes place. Based on this model, the C→D step would have occurred once for every 27 C→B→C cycles (given a 0.335-ms leash turnover time) for the 9-ms ATP synthesis-dependent 36° substep observed previously (Düser *et al*, 2009). In the absence of F_1, the F_o proton translocation rate in response to a 73-mV electric potential is two-fold greater when the potential is in the hydrolysis direction than in the synthesis direction (Wiedenmann *et al*, 2008). This difference might be explained by anisotropic behaviour of the leash.

The F_o motor has been postulated to use a Brownian ratchet mechanism that requires, first, that there are two noncolinear proton access half-channels from each side of the membrane leading to the cD61 carboxyl, and second, that rotational diffusion of the c-ring relative to subunit-a is restricted in some manner (Junge *et al*, 1997; Oster *et al*, 2000). The leash behaviour reported here can fulfill the role of the second requirement of the ratchet to restrict the rotational diffusion of the c-ring to 36°. We anticipate that the use of nanodiscs and the time resolution that is possible from the single-molecule approach presented here will have a broad application for the study of other integral membrane motors and proteins that undergo similar conformational changes.

Materials and methods

Preparation of F_1

F_1-ATPase containing a His_6 tag on the N-terminus of the β-subunit and γS193C as described previously (Greene and Frasch, 2003; York *et al*, 2007) was purified from the *E. coli* XL-10 strain. Additional details are provided in Supplementary data.

Preparation of F_oF_1

The pFV2 plasmid encoding cysteine-free F_oF_1 (Ishmukhametov *et al*, 2005) was used to introduce c2∇C, cD62G, aR210G, and a∇14 mutations with the QuikChange®II-XL Site-Directed Mutagenesis Kit (Stratagene) using oligonucleotides synthesized by Invitrogen. All mutations were confirmed by sequencing. The F_oF_1-a∇14 mutation was accidentally formed during PCR using a nonoptimal annealing temperature in the process of making the aR210G mutation.

The F_oF_1 isolation was similar to that described in Ishmukhametov *et al* (2005) with modifications. The DK8 *unc* operon deletion strain of *E. coli* (Klionsky *et al*, 1984) containing the plasmid pFV2 were grown with shaking at 37°C in 1 l of LB medium with 50 μg/ml of ampicillin. About 4–5 g wet weight of bacteria was harvested by centrifugation at 7700 *g* for 15 min at 4°C and stored as cell pellets at −80°C. Cell pellets thawed at 25°C were immediately resuspended in 100 mM KCl, 5 mM $MgCl_2$, 0.1 mM EDTA, 2.5% glycerol, and 200 mM Tris/HCl, pH 8.0, and the cells were broken using a French press at 16 000 psi. Unbroken cells were collected as a pellet at 7700 *g* for 15 min at 4°C and discarded.

All subsequent steps were performed at 4°C. The supernatant fraction containing membrane vesicles was centrifuged at 184 000 *g* for 1 h. The pellet of membranes containing F_oF_1 was resuspended in extraction buffer (EB; 100 mM NaCl, 40 mM ε-aminocaproic acid, 15 mM *p*-aminobenzamidine, 5 mM $MgCl_2$, 0.03% phosphatidylcholine, 1.0% octyl glucopyranoside, 0.5% sodium deoxycholate, 0.5% sodium cholate, 6% glycerol, 30 mM imidazole, and 50 mM Tris/HCl, pH 8.0). About 5 ml of EB was added to 1 g of membranes, which was shaken for 90 min at 4°C, then centrifuged at 184 000 *g* for 1 h. The supernatant was applied to a Ni-NTA column containing 1.5 ml of resin equilibrated with EB. The resin containing bound F_oF_1 was washed with about 20 ml of EB, and F_oF_1 was eluted with 3 ml of EB containing 180 mM imidazole. After determination of protein concentration, the solubilized F_oF_1 was immediately incorporated into nanodiscs.

Preparation of n-F_oF_1

The MSP construct MSP1E3D1 was used that is composed of scaffold protein contains three 22-mer amphipathic helices and a cleavable his-tag as the result of an introduced TEV protease site to facilitate purification (Denisov *et al*, 2004; Bayburt *et al*, 2007). Nanodiscs formed from this construct contain a lipid bilayer that is about 13 nm in diameter surrounded by a double belt of the MSP helices. The His-tag of the purified MSP-1E3D1 was cleaved by overnight incubation with TEV protease (at 25:1 ratio, w/w) at 25°C and passed through a Ni-NTA column. We assembled n-F_oF_1 by mixing MSP in Buffer D (50 mM Tris, pH 8.0, 100 mM NaCl, 4 mM 4-aminobenzamidine, 5 mM $MgCl_2$ and 5% (v/v) glycerol) with

10% sodium cholate in Buffer D, and F_oF_1 in Elution Buffer to achieve a 1:7 molar ratio of F_oF_1:MSP in 1% sodium cholate with a final volume not exceeding 1 ml, and adjusted with Buffer D. To make biotinylated n-F_oF_1, a 10-fold molar excess of biotin maleimide was added to this mixture. The mixture was incubated at 4°C for 15 min with gentle shaking, then passed through a 2-ml Sephadex G-50 column equilibrated with Buffer D from which 3 ml of effluent were collected. The effluent was diluted with Buffer D to 6 ml to decrease the imidazole concentration to <30 mM, and passed through a 1.5-ml Ni-NTA column. The column was washed with 15 ml of Buffer D and eluted with Buffer D, containing 150 mM imidazole. The yield of n-F_oF_1 was ~60–70% of the amount of F_oF_1 starting material as measured with the BCA protein assay (Sigma).

2D electrophoresis

Proteins (6 μg total per sample) were first separated on a 5–15% native polyacrylamide gradient gel for 4.5 h at room temperature. The gel slice with the single-dominant band was excised from the gel and transferred to a glass plate, which was covered with 12% denaturing gel (SDS–PAGE). The sample was run for 4.5 h at 25°C and silver stained as described (Nesterenko *et al*, 1994).

ATP hydrolysis assay and DCCD modification conditions

To modify the enzyme by DCCD, 10–30 μg of protein was incubated with 50 μM DCCD at pH 6.5. at 28°C in a 2-ml cuvette for 30 min. This solution was diluted into the reaction mixture used to measure ATPase activity. The rate of ATP hydrolysis was measured with an ATP-regenerating coupled assay that resulted in a final concentration of 50 mM Tris–HCl (pH 8.0), 10 mM KCl, 2.5 mM phosphoenolpyruvate, 0.3 mM NADH, 50 μg/ml pyruvate kinase, 50 μg/ml lactate dehydrogenase, and 2 mM $MgCl_2$ and 1 mM ATP. The rate was determined as the change in absorbance at 340 nm using a Cary 100 spectrophotometer with Peltier temperature control. ATPase-driven proton translocation was measured by ACMA quenching using F_oF_1 containing membranes as described (Ishmukhametov *et al*, 2005).

Single-molecule studies

To assemble n-F_oF_1 with a nanorod on the slide, the slide was spotted with 5 μl of about 85 μg/ml of n-F_oF_1 and incubated for 5 min. The slide was washed with assay buffer (10 mM KCl and 50 mM Tris, pH 8.0) for 30 s, and excess liquid was removed. Immobilized n-F_oF_1 was exposed to 5 μl avidin-coated gold nanorods prepared as described (Spetzler *et al*, 2006) for 5 min, then washed with assay buffer. After excess liquid was removed, 5 ml of assay buffer containing the desired amount of PEG400, 2 mM ATP and 1 mM $MgCl_2$ was added, a cover slip was applied, and the slide was placed on the microscope.

Rotation measurements were performed as described in Spetzler *et al* (2009) and Spetzler *et al* (2006) using a Leica DMIRE II inverted dark field microscope illuminated with a Sutter LB-17 Xenon light source with a custom Chroma cold mirror coupled with a series 2000 Lumatec light guide to deliver 400–925 nm collimated light to the dark field condenser. Light not scattered by gold nanorods was blocked by an iris in the ×63 variable aperture objective. Colour photos of fields of view under the microscope were obtained with a Zeiss Axiocam HSC series-2 camera with a refresh rate of 53 fps.

To measure transitions, a nanorod observed to blink red and green was positioned to a 100-μm pinhole to allow light scattered from that nanorod passed through a polarizing filter and a high pass 600 nm cutoff filter (to permit only red light), and focused onto a single-photon counting avalanche photodiode (Perkin Elmer SPCM-AQR-15) that has a dark count of ~50 photons s^{-1} with a temporal resolution of 50 ns. Detector output was fed to a National Instruments DAQ PCI-6602 counter/timer board. Photons were recorded and binned into different time intervals that provided rotational data with various time resolutions. The rotation of each molecule was monitored for 50 s at a data acquisition speed of 100–200 kHz to provide a minimal time resolution of 20–10 μs. Custom software was written in LabView 7.1 to control data acquisition and storage. Additional custom software was written in Matlab 6.5 to compute transition times.

Supplementary data

Supplementary data are available at *The EMBO Journal* Online (http://www.embojournal.org).

Acknowledgements

We thank Stephen Sligar for providing MSP1E3D1 and Yelena Grinkova for advice in its handling. We thank R Fillingame, W Junge, P Gräber, and P Dimroth for helpful comments in the preparation of this manuscript. This project was supported by R01GM50202 to WDF. The content is solely the responsibility of the authors and does not necessarily represent the official views of the NIGMS or the NIH.

Conflict of interest

The authors declare that they have no conflict of interest.

References

Angevine CM, Herold KA, Fillingame RH (2003) Aqueous access pathways in subunit a of rotary ATP synthase extend to both sides of the membrane. *Proc Natl Acad Sci USA* **100** (23)**:** 13179–13183

Angevine CM, Herold KA, Vincent OD, Fillingame RH (2007) Aqueous access pathways in ATP synthase subunit a. Reactivity of cysteine substituted into transmembrane helices 1, 3, and 5. *J Biol Chem* **282:** 9001–9007

Bayburt TH, Leitz AJ, Xie G, Oprian DD, Sligar SG (2007) Transducin activation by nanoscale lipid bilayers containing one and two rhodopsins. *J Biol Chem* **282:** 14875–14881

Börsch M, Diez M, Zimmermann B, Reuter R, Gräber P (2002) Stepwise rotation of the gamma-subunit of EF_oF_1-ATP synthase observed by intramolecular single-molecule fluorescence resonance energy transfer. *FEBS Lett* **527:** 147–152

Boyer PD (1997) The ATP synthase–a splendid molecular machine. *Annu Rev Biochem* **66:** 717–749

Breen GA, Miller DL, Holmans PL, Welch G (1986) Mitochondrial DNA of two independent oligomycin-resistant Chinese hamster ovary cell lines contains a single nucleotide change in the ATPase 6 gene. *J Biol Chem* **261:** 11680–11685

Dautant A, Velours J, Giraud MF (2010) Crystal structure of the Mg.ADP-inhibited state of the yeast F_1c10-ATP synthase. *J Biol Chem* **285:** 29502–29510

Denisov IG, Grinkova YV, Lazarides AA, Sligar SG (2004) Directed self-assembly of monodisperse phospholipid bilayer nanodiscs with controlled size. *J Am Chem Soc* **126:** 3477–3487

Düser MG, Zarrabi N, Cipriano DJ, Ernst S, Glick GD, Dunn SD, Börsch M (2009) 36 degrees step size of proton-driven c-ring rotation in F_oF_1-ATP synthase. *EMBO J* **28:** 2689–2696

Elston T, Wang H, Oster G (1998) Energy transduction in ATP synthase. *Nature* **391:** 510–513

Feniouk BA, Junge W (2008) Proton translocation and ATP synthesis by the F_oF_1-ATPase of purple bacteria. In *The Purple Phototrophic Bacteria*, Hunter CN, Daldal F, Thurnauer MC, Beatty JT (eds), Vol. 24, pp 475–494. The Netherlands: Springer

Fillingame RH, Jiang W, Dmitriev OY, Jones PC (2000) Structural interpretations of F_o rotary function in the *Escherichia coli* F_1F_o ATP synthase. *Biochim Biophys Acta* **1458:** 387–403

Fillingame RH, Peters LK, White LK, Mosher ME, Paule CR (1984) Mutations altering aspartyl-61 of the omega subunit (uncE protein) of *Escherichia coli* H^+ -ATPase differ in effect on coupled ATP hydrolysis. *J Bacteriol* **158:** 1078–1083

Fischer S, Etzold C, Turina P, Deckers-Hebestreit G, Altendorf K, Gräber P (1994) ATP synthesis catalyzed by the ATP synthase of *Escherichia coli* reconstituted into liposomes. *Eur J Biochem* **225:** 167–172

Franklin MJ, Brusilow WS, Woodbury DJ (2004) Determination of proton flux and conductance at pH 6.8 through single F_o sectors from *Escherichia coli*. *Biophys J* **87:** 3594–3599

Greene MD, Frasch WD (2003) Interactions among gamma R268, gamma Q269, and the beta subunit catch loop of *Escherichia coli*

F_1-ATPase are important for catalytic activity. *J Biol Chem* **278:** 51594–51598

Hornung T, Ishmukhametov R, Spetzler D, Martin J, Frasch WD (2008) Determination of torque generation from the power stroke of *Escherichia coli* F_1-ATPase. *Biochim Biophys Acta* **1777:** 579–582

Ishmukhametov RR, Galkin MA, Vik SB (2005) Ultrafast purification and reconstitution of His-tagged cysteine-less *Escherichia coli* F_1F_o ATP synthase. *Biochim Biophys Acta* **1706:** 110–116

Ishmukhametov RR, Pond JB, Al-Huqail A, Galkin MA, Vik SB (2008) ATP synthesis without R210 of subunit a in the *Escherichia coli* ATP synthase. *Biochim Biophys Acta* **1777:** 32–38

Jiang W, Fillingame RH (1998) Interacting helical faces of subunits a and c in the F_1F_o ATP synthase of *Escherichia coli* defined by disulfide cross-linking. *Proc Natl Acad Sci USA* **95:** 6607–6612

Jiang WP, Hermolin J, Fillingame RH (2001) The preferred stoichiometry of c subunits in the rotary motor sector of *Escherichia coli* ATP synthase is 10. *Proc Natl Acad Sci USA* **98:** 4966–4971

John UP, Nagley P (1986) Amino acid substitutions in mitochondrial ATPase subunit 6 of *Saccharomyces cerevisiae* leading to oligomycin resistance. *FEBS Lett* **207:** 79–83

Junge W, Lill H, Engelbrecht S (1997) ATP synthase: an electrochemical transducer with rotatory mechanics. *Trends Biochem Sci* **22:** 420–423

Kaim G, Dimroth P (1998) ATP synthesis by the F_1F_o ATP synthase of *Escherichia coli* is obligatorily dependent on the electric potential. *FEBS Lett* **434:** 57–60

Kaim G, Prummer M, Sick B, Zumofen G, Renn A, Wild UP, Dimroth P (2002) Coupled rotation within single F_oF_1 enzyme complexes during ATP synthesis or hydrolysis. *FEBS Lett* **525:** 156–163

Klionsky DJ, Brusilow WS, Simoni RD (1984) *In vivo* evidence for the role of the epsilon subunit as an inhibitor of the proton-translocating ATPase of *Escherichia coli*. *J Bacteriol* **160:** 1055–1060

Lightowlers RN, Howitt SM, Hatch L, Gibson F, Cox GB (1987) The proton pore in the *Escherichia coli* F_oF_1-ATPase: a requirement for arginine at position 210 of the a-subunit. *Biochim Biophys Acta* **894:** 399–406

Meier T, Krah A, Bond PJ, Pogoryelov D, Diederichs K, Faraldo-Gomez JD (2009) Complete ion-coordination structure in the rotor ring of Na^+-dependent F-ATP synthases. *J Mol Biol* **391:** 498–507

Moore KJ, Angevine CM, Vincent OD, Schwem BE, Fillingame RH (2008) The cytoplasmic loops of subunit a of *Escherichia coli* ATP synthase may participate in the proton translocating mechanism. *J Biol Chem* **283:** 13044–13052

Moore KJ, Fillingame RH (2008) Structural interactions between transmembrane helices 4 and 5 of subunit a and the subunit c ring of *Escherichia coli* ATP synthase. *J Biol Chem* **283:** 31726–31735

Nesterenko MV, Tilley M, Upton SJ (1994) A simple modification of Blum's silver stain method allows for 30 minute detection of proteins in polyacrylamide gels. *J Biochem Biophys Methods* **28:** 239–242

Nishio K, Iwamoto-Kihara A, Yamamoto A, Wada Y, Futai M (2002) Subunit rotation of ATP synthase embedded in membranes: a or beta subunit rotation relative to the c subunit ring. *Proc Natl Acad Sci U S A* **99:** 13448–13452

Noji H, Hasler K, Junge W, Kinosita Jr K, Yoshida M, Engelbrecht S (1999) Rotation of Escherichia coli F_1-ATPase. *Biochem Biophys Res Commun* **260:** 597–599

Oster G, Wang H, Grabe M (2000) How F_o-ATPase generates rotary torque. *Philos Trans R Soc Lond B Biol Sci* **355:** 523–528

Pänke O, Gumbiowski K, Junge W, Engelbrecht S (2000) F-ATPase: specific observation of the rotating c subunit oligomer of EF_oEF_1. *FEBS Lett* **472:** 34–38

Pogoryelov D, Yildiz O, Faraldo-Gomez JD, Meier T (2009) High-resolution structure of the rotor ring of a proton-dependent ATP synthase. *Nat Struct Mol Biol* **16:** 1068–1073

Ray MK, Connerton IF, Griffiths DE (1988) DNA sequence analysis of the Olir2-76 and Ossr1-92 alleles of the Oli-2 region of the yeast *Saccharomyces cerevisiae*. Analysis of related amino-acid substitutions and protein-antibiotic interaction. *Biochim Biophys Acta* **951:** 213–219

Sabbert D, Engelbrecht S, Junge W (1996) Intersubunit rotation in active F-ATPase. *Nature* **381:** 623–625

Sambongi Y, Iko Y, Tanabe M, Omote H, Iwamoto-Kihara A, Ueda I, Yanagida T, Wada Y, Futai M (1999) Mechanical rotation of the c subunit oligomer in ATP synthase (F_oF_1): direct observation. *Science* **286:** 1722–1724

Senior AE, Nadanaciva S, Weber J (2002) The molecular mechanism of ATP synthesis by F_1F_o-ATP synthase. *Biochim Biophys Acta* **1553:** 188–211

Sielaff H, Rennekamp H, Wachter A, Xie H, Hilbers F, Feldbauer K, Dunn SD, Engelbrecht S, Junge W (2008) Domain compliance and elastic power transmission in rotary FOF1-ATPase. *Proc Natl Acad Sci U S A* **105:** 17760–17765

Sönnichsen C, Alivisatos AP (2005) Gold nanorods as novel nonbleaching plasmon-based orientation sensors for polarized single-particle microscopy. *Nano Lett* **5:** 301–304

Spetzler D, Ishmukhametov R, Hornung T, Day LJ, Martin J, Frasch WD (2009) Single molecule measurements of F_1-ATPase reveal an interdependence between the power stroke and the dwell duration. *Biochemistry* **48:** 7979–7985

Spetzler D, York J, Daniel D, Fromme R, Lowry D, Frasch W (2006) Microsecond time scale rotation measurements of single F_1-ATPase molecules. *Biochemistry* **45:** 3117–3124

Steed PR, Fillingame RH (2009) Aqueous accessibility to the transmembrane regions of subunit c of the *Escherichia coli* F_1F_o ATP synthase. *J Biol Chem* **284:** 23243–23250

Stock D, Leslie AG, Walker JE (1999) Molecular architecture of the rotary motor in ATP synthase. *Science* **286:** 1700–1705

Turina P, Samoray D, Gräber P (2003) H^+/ATP ratio of proton transport-coupled ATP synthesis and hydrolysis catalysed by CF_oF_1-liposomes. *EMBO J* **22:** 418–426

Ueno H, Suzuki T, Kinosita K, Yoshida M (2005) ATP-driven stepwise rotation of F_oF_1,-ATP synthase. *Proc Natl Acad Sci USA* **102:** 1333–1338

Vik SB, Cain BD, Chun KT, Simoni RD (1988) Mutagenesis of the alpha subunit of the F_1F_o-ATPase from *Escherichia coli*. Mutations at Glu-196, Pro-190, and Ser-199. *J Biol Chem* **263:** 6599–6605

Vollmar M, Schlieper D, Winn M, Buchner C, Groth G (2009) Structure of the c14 rotor ring of the proton translocating chloroplast ATP synthase. *J Biol Chem* **284:** 18228–18235

Weber J, Senior AE (1997) Catalytic mechanism of F_1-ATPase. *Biochim Biophys Acta* **1319:** 19–58

Wiedenmann A, Dimroth P, von Ballmoos C (2008) Deltapsi and DeltapH are equivalent driving forces for proton transport through isolated F_o complexes of ATP synthases. *Biochim Biophys Acta* **1777:** 1301–1310

Yasuda R, Noji H, Kinosita Jr K, Yoshida M (1998) F_1-ATPase is a highly efficient molecular motor that rotates with discrete 120 degree steps. *Cell* **93:** 1117–1124

Yasuda R, Noji H, Yoshida M, Kinosita K, Itoh H (2001) Resolution of distinct rotational substeps by submillisecond kinetic analysis of F_1-ATPase. *Nature* **410:** 898–904

York J, Spetzler D, Hornung T, Ishmukhametov R, Martin J, Frasch WD (2007) Abundance of *Escherichia coli* F_1-ATPase molecules observed to rotate via single-molecule microscopy with gold nanorod probes. *J Bioenerg Biomembr* **39:** 435–439

Zhang D, Vik SB (2003a) Close proximity of a cytoplasmic loop of subunit a with c subunits of the ATP synthase from *Escherichia coli*. *J Biol Chem* **278:** 12319–12324

Zhang D, Vik SB (2003b) Helix packing in subunit a of the *Escherichia coli* ATP synthase as determined by chemical labeling and proteolysis of the cysteine-substituted protein. *Biochemistry* **42:** 331–337